INVESTIGATION OF THE ARIANE-5 NOZZLE SECTION BY DES

H. Lüdeke
DLR, Institute of Aerodynamics and Flow Technology , Lilienthalplatz 7, D-38108 Braunschweig
Tel. +49 (531) 295-3315, e-mail: Heinrich.Luedeke@dlr.de

Abstract

The modeling of unsteady side loads induced by the interaction of flow separation inside nozzles and launcher wake will play an important role for the design of future propulsion systems. The simulation of this phenomenon, called buffeting coupling, is one of the main challenges during ascent. To investigate the whole nozzle flow field, basic studies of generic configurations by advanced turbulence models are necessary. For this reason the validation of the Detached Eddy Simulation implemented in the τ-code for an axisymmetric supersonic cylinder configuration are carried out. Furthermore unsteady simulations of the Ariane-5 nozzle section are investigated and validated by wind tunnel data.

Introduction

One challenge of numerical investigations of unsteady super- and hypersonic flow fields is the study of turbulent wake flow and the interaction with nozzle sections at complex vehicle configurations. A recent approach is the technique of detached-eddy simulation (DES) proposed by Spalart et.al [1,2]. Detached-eddy simulation is a hybrid approach for the modeling of turbulent flow fields at complex geometries. The idea is to combine the best features of Reynolds-averaged Navier-Stokes (RANS) and the large eddy simulation (LES) to predict massively separated unsteady flow fields at high Reynolds-numbers. As a basic validation case for supersonic DES the unsteady axisymmetric flow fields in the wake of a blunt cylinder at M = 2.4 and high Reynolds numbers is chosen. In the following realistic simulations of the Ariane-5 nozzle section are carried out. The typical time averaged flow field for this configuration is shown in Fig. 1 with pressure contours and streamlines. The large turning angle behind the base causes separation and a region of reverse flow as visible in the wake.

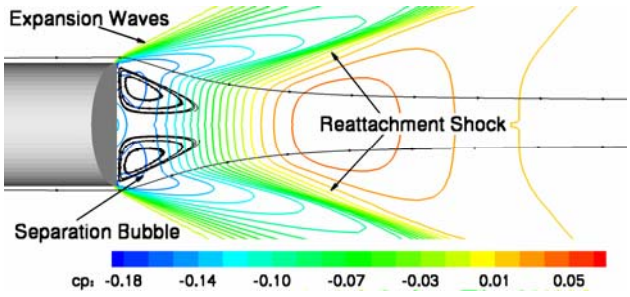

Fig. 1: Flow topology of axisymmetric base flow and C_p distribution at M=2.4.

The point along the axis of symmetry where the streamwise velocity is zero is considered to be the shear layer reattachment point. In this region the flow is forced to turn along the axis of symmetry causing a reattachment shock to be formed. Experimentally the detailed data base, provided by Herrin and Dutton [3], is used. All simulations were carried out by the hybrid structured-unstructured DLR-τ-code which is extensively validated for sub- trans- and hypersonic cases [4].

Aside from grid studies, investigations of different low-Reynolds number modifications of the LES part proposed by Breuer [6] were applied for both grids [7]. In the wake the turbulent kinetic energy and turbulent intensities in radial and streamwise direction was successfully compared with the measurements. Furthermore base pressure level and centerline velocity was compared with experimental data [3].

Finally steady as well as unsteady Ariane-5 simulations under turbulent conditions are carried out for transonic wind tunnel conditions including jet flow and launcher wake and power spectral densities.

Numerical simulation tools

The CFD computations for this study are performed with the hybrid structured/unstructured DLR-Navier-Stokes Solver τ, which is validated for a wide range of steady and unsteady sub- trans- and hypersonic flow cases [4]. The τ-code is a second order finite-volume flow solver for the Euler and Navier-Stokes equations in the integral form. Different numerical schemes like cell-centered for sub- and transonic flow and AUSMDV for super- and hypersonic flow conditions are implemented. Second-order accuracy for upwind schemes is obtained by the MUSCL extrapolation, in order to allow the capturing of strong shocks and contact discontinuities. A three-stage Runge-Kutta scheme is used to advance the solutions in time for steady flow fields. For convergence acceleration local time stepping, implicit residual smoothing and full multigrid are optional.

For fast and accurate transient flow simulations a Jameson type dual time stepping scheme, is implemented as an implicit algorithm and not restricted in the choice of the smallest timestep in the flow field. To overcome this limit the time derivative in the Navier-Stokes equations is discretized by a second order backwards difference, resulting in a non-linear equation system which converges towards the subsequent timestep by using an inner pseudo-time. Within this inner loop all mentioned acceleration techniques are applicable.

Several one- and two equation turbulence models are available for steady simulations. In the presented RANS-cases the one-equation Spalart-Allmaras (SA) model is used which is briefly described in the following. The model defines the eddy viscosity field as

$$\mu_t = \rho \nu_t = \rho \tilde{\nu} f_{\nu 1}$$

with ρ as the density, ν_t as the turbulent kinematic viscosity and $f_{\nu 1}$ as a near wall-function that guarantees linear behavior of the turbulent transport quantity $\tilde{\nu}$ near walls:

$$f_{\nu 1} = \left(\frac{\chi^3}{\chi^3 + c_{\nu 1}^3} \right)$$

$$\chi = \frac{\tilde{\nu}}{\nu}$$

with ν as the molecular viscosity.

The distribution of the transport quantity $\tilde{\nu}$ is determined by the solution of

$$\frac{D(\rho\tilde{\nu})}{Dt} = \underbrace{c_{b1}\tilde{S}\rho\tilde{\nu}}_{P} - \underbrace{C_{w1}f_w\rho\left(\frac{\tilde{\nu}}{d}\right)^2}_{D} + \underbrace{\frac{\rho}{\sigma}\left\{\nabla[(\nu+\tilde{\nu})\nabla\tilde{\nu}] + c_{b2}(\nabla\tilde{\nu})^2\right\}}_{DF}$$

with d as the wall distance. This transport equation contains phenomenological models of production *P*, destruction *D* and diffusion *DF*. The destruction term D is needed to model the blocking effects near walls. In the production term *P* a modified vorticity $\tilde{S}$ appears that maintains the linear behavior of the model near walls:

$$\tilde{S} = S + \frac{\tilde{\nu}}{k^2 d^2} f_{\nu 2}$$

$$f_{\nu 2} = 1 - \frac{\chi}{1+\chi f_{\nu 1}}$$

The function $f_{\nu 2}$ is constructed in a way that the vorticity S maintains its log-layer behavior all the way to the wall. The destruction term

$$D = C_{w1} f_w \rho\left(\frac{\tilde{\nu}}{d}\right)^2$$

is constructed by using the wall function f_w:

$$f_w = g\left[\frac{1+c_{w3}^6}{g^6 + c_{w3}^6}\right]$$

$$g = r + c_{w2}\left(r^6 - r\right)$$

$$r = \frac{\tilde{\nu}}{Skd^2}$$

The different model constants $c_{\nu 1}, c_{b1}, c_{b2}, c_{w1}, c_{w3}$ are determined by experimental data and analytical solutions and are well known for turbulent flowfields [2].

During the last years more recent turbulence models like DES are implemented [8]. DES is a hybrid RANS-LES approach that bases on a modification of the wall distance term in the SA model. While RANS is used in the unsteady boundary layer flow where it performs reasonable results, LES is used in separated regions where relevant turbulent scales can be modeled. The switching between RANS and LES bases on a characteristic length scale, chosen to be proportional with Δ which is the largest cell dimension:

$$\Delta = \max(\Delta x, \Delta y, \Delta z)$$

For the standard DES formulation the wall distance d in the SA model is replaced by $\tilde{d}$ where $\tilde{d}$ is defined as:

$$\tilde{d} = \min(d, C_{DES}\Delta)$$

with C_{DES} as a constant calibrated by using isotropic turbulence. In this mode a local equilibrium between production and destruction term in the SA model is expected. This local balance leads to the relation which is very similar to the relation $\tilde{\nu} \propto \tilde{S}\cdot\tilde{d}^2$ in the Smagorinsky model which is $\nu_t \propto S\cdot\tilde{d}^2$. Consequently the only difference between SA-DES in LES-mode and the original Smagorinsky model lies in the SA-wall-functions $f_{\nu 1}, f_{\nu 2}, f_w$, hidden in $\tilde{\nu}$ and $\tilde{S}$. The influence of these functions is small for high Reynolds numbers, and disappears for a large wall distance. However in LES mode the wall distance is substituted by the small filter-width, so the impact of these function especially in free shear flow can be significant.

In order to get the exact Smagorinsky model, Breuer [6] expected the following conditions to be satisfied in the LES region $(d \rangle C_{DES}\Delta)$:

$$f_{\nu 1} = 1$$

$$f_{\nu 2} = 0$$

$$f_w = 1$$

These functions can be easily included in the original DES formulation, and the modi-

fication is optional in the recent τ-code version. The impact of this correction was already shown in [7].

Grid generation

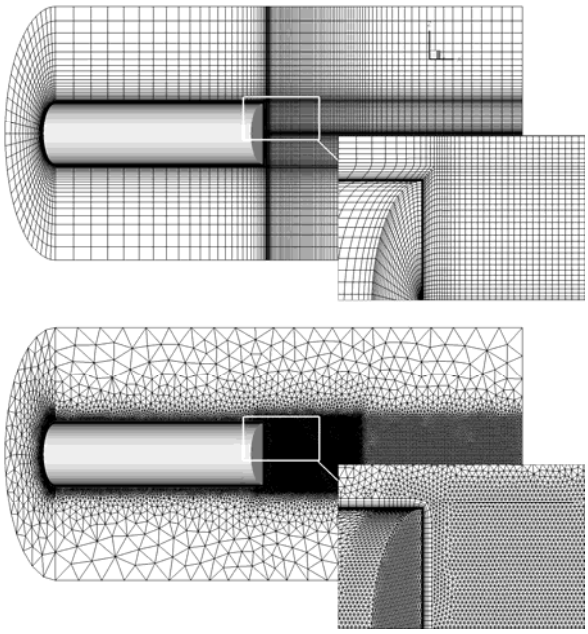

Fig. 2: Hexahedral and tetrahedral grid for the cylinder wake

For the axisymmetric cylinder-configuration structured as well as unstructured grids have been generated at a different resolution of the turbulent wake. They are designed with a similar resolution used by Forsythe and Sqires [5]. Especially the near wake of the cylinder is refined extensively, following the recommendation of Spalart [1].

For basic studies of compressible DES a coarse hexahedral grid with axisymmetric character, shown on top of Fig. 2, is generated. For grid convergence studies also a hybrid unstructured grid is used (Fig. 2 bottom). While the hexahedral grid has only 360.000 cells, to study the accuracy of the numerical schemes, the hybrid grid with about 2.000.000 cells provides a significantly improved resolution in the shear layer and wake, but on the other hand an increase in computational cost.

The computational Ariane-5 grid is shown in Fig. 3. For the reason of extensively time consuming DES simulations, the hexahedral grid provided by ESA with only $2 \cdot 10^6$ cells for the half configuration is used. For the investigations the forebody part of the launcher is computed separately as a steady flowfield, and the connecting plane of both grid-parts is used as a steady inflow-plane for the transient simulation.

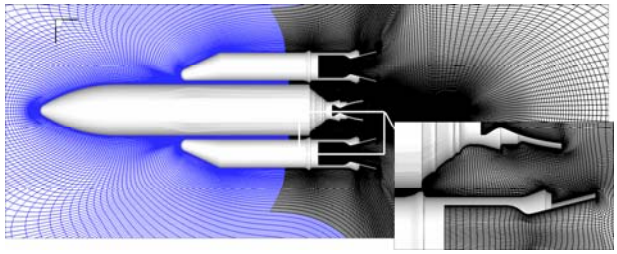

Fig. 3: Symmetry plane of the Ariane-5 hexahedral grid, fore and afterbody

Computational results

Axisymmetric base flow

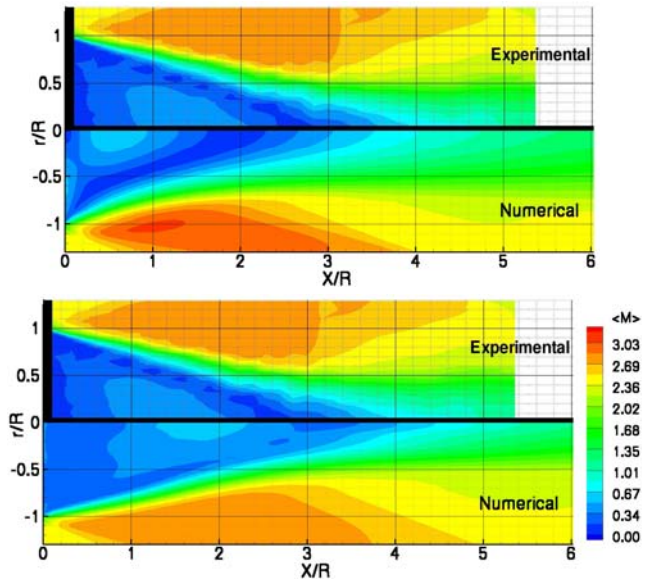

Fig. 4: Averaged Mach contours behind cylinder base. Top: RANS on hexahedral grid, bottom: averaged Mach contour of DES . Experiments from [3].

For both grids the standard DES model, suggested by Spalart [1] with a slightly modified filter-length is used. Instead of the maximum cell diameter the third root of the cell volume, typically used for LES simulations, is chosen in the DES-region which is defined by the standard procedure. The advantage of this choice is a better treatment of highly stretched cells in the hexahedral grid. It has to be noted, that the switching between RANS and LES is kept at the same position as before, so the whole boundary layer is still computed in RANS-mode. The test conditions for the compressible base flow are taken from [5] at M_∞ = 2.46, $Re_\infty = 45 \cdot 10^6$/m, U_∞ = 593.8 m/s and a cylinder radius of 31.75 mm. The averaged Mach number distribution in the cylinder wake agrees well with the experimental data by Herrin and Dutton [3], as shown in Fig. 4 for RANS and DES simulation.

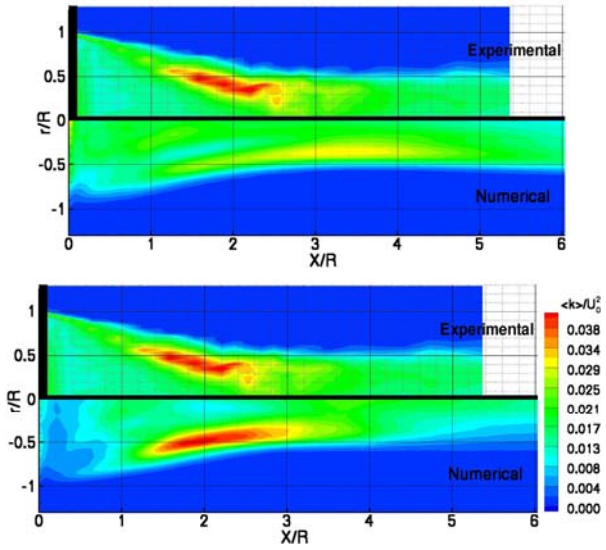

Fig. 5: Resolved turbulent kinetic energy behind cylinder base. Top: DES on hexahedral grid, Bottom: DES on tetrahedral grid. Experiments from [3].

For this insensitive quantity even steady RANS simulations show reasonable results, although the agreement with DES is much better. Also higher statistical moments, like the resolved turbulent kinetic energy $k = 0.5 \cdot (\sigma u^2 + \sigma v^2 + \sigma w^2)$ are compared, where σ is the standard deviation over time of the respective velocity component.

The result of k for the standard DES model is shown in Fig. 5 on the left hand side with the same k-distribution in the shear layer. The results could be improved by using the refined unstructured grid, as shown on the right hand side. With the improved resolution of the free shear layer it is possible to get a much better agreement of the k-distribution in that region as expected physically.

Main advantages of the DES-approach are shown by a comparison between simulated and experimental pressure distribution at the cylinder-base and the centerline velocity for RANS- and DES-calculations (Fig. 6).

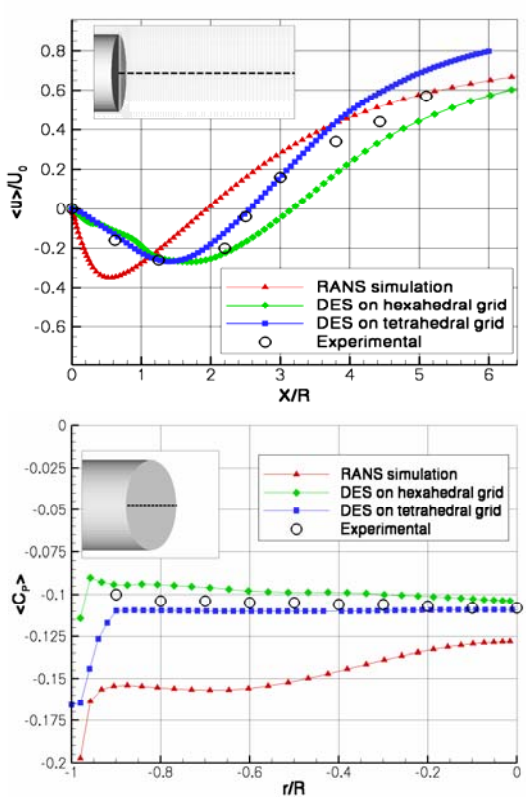

Fig. 6: Averaged centerline velocity and base pressure for structured and unstructured grid. Experiments from [3].

As visible the mean pressure level predicted by RANS is globally smaller than the experimental data while the DES results generated on hexa- and tetrahedral grid agree well

with the experiments. This is also true for the centerline velocity, although in a certain distance from the base the quality of the results decrease due to an insufficient grid resolution. This distance varies between X/R=2 for the hexahedral- and X/R=4 for the tetrahedral grid. In both cases this is the beginning of the area, where the grids become coarser.

Ariane-5 results

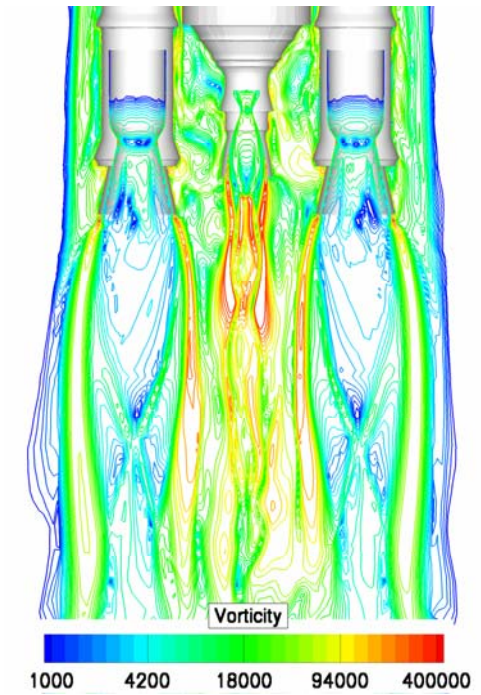

Fig. 7: Ariane-5 DES simulation: snapshot of vorticity in the symmetry plane.

For the calculations of the Ariane-5 nozzle-flowfield, wind tunnel conditions of M=0.8, Re=$11 \cdot 10^6$/m are chosen. For these conditions detailed experimental studies of NLR and ESA are carried out. The computational Ariane-5 grid was already shown in Fig. 3. As mentioned the forebody part of the launcher is computed separately to get a steady inflow-plane for the transient simulation. The density distribution for the steady RANS-result (see [7]) compares well with the experimental results from [8].

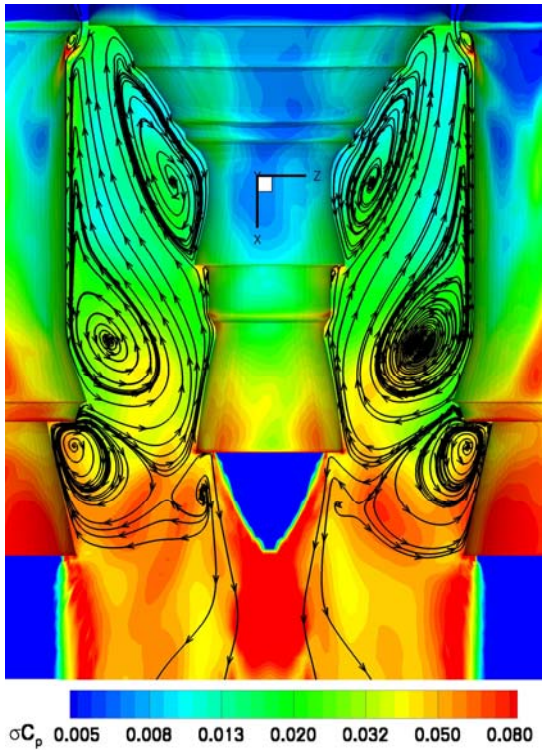

Fig. 8: Ariane-5 DES simulation: Root mean square value of C_P and time averaged streamlines.

The DES results show complex interactions between the different nozzle plumes of boosters and central nozzle, which is visible especially for the vorticity contours (Fig. 7). A cut-out of the flowfield between the three nozzles is shown in Fig. 8 with the RMS-value of C_p and the streamlines of the averaged flowfield. It shows the system of separations and vortices resulting from the interaction of the nozzle flow and the jet coming out of the gap between boosters and main stage.

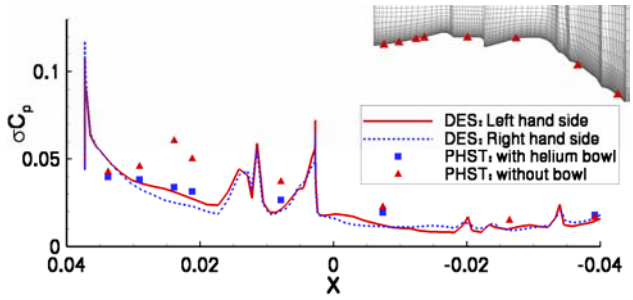

Fig. 9: Ariane-5 DES simulations: RMS values of pressure coefficient along EPC nozzle.

This interaction is probably also responsible for the main aerodynamic frequencies dominating the pressure distribution.

In Fig. 9 the root mean square values of C_p along the surface of the central EPC nozzle section are compared with experimental data from the NLR PHST facility. While the wind tunnel model consists of a helium bowl aside of the nozzle, the DES calculations are carried out on a symmetric configuration without bowl. While the red triangles show kulite signals on the left hand model side where the bowl is mounted, the blue squares represent data of the opposite part. Surprisingly the numerical results agree better with the part including the bowl. This discrepancy can be explained by a shadowing influence of the bowl on the vortices in the flow field. Furthermore due to the subsonic character of the flow, the wake of the bowl may have a strong influence on the opposite part of the launcher. To verify these statements, of course further simulations, including the He-bowl have to be carried out in future studies.

Conclusion

The present study investigates unsteady axisymmetric flow fields in the wake of a blunt cylinder at M_∞=2.4 and the wake of the Ariane-5 in the nozzle section under wind tunnel conditions. The time accurate Detached Eddy Simulations have shown very good agreement with experimental data of base flow especially for the prediction of base pressure and centerline velocity especially for the tetrahedral grid with improved shear layer resolution. Also other turbulent quantities like the diagonal elements of the Reynolds-stress tensor and the turbulent kinetic energy compare well with the measured data. Finally the technique was applied on the Ariane-5 under transonic conditions. Simulation results are shown for this configuration. The results agree well with the experimental database provided by the NLR/ESA experiments.

References

1. P.R. Spalart: Young-Person's Guide to Detached- Eddy Simulation Grids. NASA/CR-2001-211032, (2001).
2. P.R. Spalart, S.R. Allmaras: A One Equation Turbulence Transport Model for Aerodynamic Flows, La Recherche Aérospaciale, No. 1, 1994, pp. 5-21.
3. 4. J.L. Herrin, J.C. Dutton: Supersonic Base flow Experiments in the Near Wake of a Cylindrical Afterbody. AIAA Journal, Vol 32, No. 1, January 1994 (1994).
4. A. Mack, V. Hannemann: Validation of the unstructured DLR-TAU-Code for Hypersonic Flows, AIAA 2002-3111, (2002).
5. J.R. Forsythe, K.A. Hoffmann, K.D. Squires: Detached-Eddy Simulation with compressibility Corrections Applied to a Supersonic Axisymmetric Base Flow. AIAA 02-0586 (2002).
6. M. Breuer, N. Jovicic, K. Mazaev: Comparison of DES, RANS and LES for the separated flow around a flat plate at high incidence. Int. J. Numer. Meth. Fluids, 41: pp 357-388 (2003).
7. H. Lüdeke, A. Filimon: Investigations of Transient Flow Phenomena at the ARIANE-5 Propulsion System During Ascent. 5th European Symposium on Aerothermodynamics for Space Vehicles, Cologne, November 8-11 (2004).
8. J. Muylaert, W. Berry: Aerodynamics for Space Vehicles- ESA's Activities and the Challenges, ESA bulletin 96 (November 1998)
9. H. Wong, J. Meijer, R. Schwane: Theoretical and Experimental Investigations on Ariane5 Base-Flow Buffeting. 5th European Symposium on Aerothermodynamics for Space Vehicles, Cologne, November 8-11 (2004).